Organisation and complexation of mono- and bis-beta-cyclodextrins without chromophores with a fluorescence-sensitive probe in aqueous solutions

Organization and complexation of *mono*- and *bis*βcyclodextrins without chromophores with a fluorescence sensitive probe in aqueous solutions

Thais Carmona[#], Marina Caporaso†, Katia Martina†, Giancarlo Cravotto†, Francisco Mendicuti[#]*

[#] Departamento de Química Analítica, Química Física e Ingeniería Química, Universidad de Alcalá. 28871 Alcalá de Henares. Madrid. Spain.

† Dipartimento di Scienza e Tecnologia del Farmaco and NIS - Centre for Nanostructured Interfaces and Surfaces, University of Turin. Via P. Giuria, 9, 10125 Turin, Italy

CORRESPONDING AUTHOR (*):

Francisco Mendicuti

Phone number: 34-91-8854672

Fax number: 34-91-8854763

E-mail:francisco.mendicuti@uah.es

Abstract

The behaviour of *mono*- and *bis*-βCD derivatives, namely 6^{I}-deoxy-6^{I}-[4-(hept-6-ynyl)-1*H*-1,2,3-triazolyl]-β-cyclodextrin and 1,5-*bis*((1-(6^{I}-deoxy-β-cyclodextrin-6^{I}-yl)-1*H*-1,2,3-triazol-4-yl)methoxy) pentyl, whose appended groups and inter-CD linkers respectively do not contain any chromophore, as well as their complexation with dimethyl 2,6-naphthalenedicarboxylate (DMN), a fluorescent polarity sensitive probe in aqueous solutions were investigated. Steady-state, time-resolved fluorescence, circular dichroism techniques, Molecular Mechanics (MM) and Molecular Dynamics (MD) simulations were employed. DMN appeared to slightly interact with the *mono*-βciclodextrin and only unstable non-covalent dimers were formed. On the contrary, stable 1:1 and 2:1 stoichiometry complexes were obtained with *bis*-βciclodextrin and DMN. A certain cooperativity due to the presence of both cavities and the linker favoured the formation of the complex 2:1 DMN:CD. DMN appeared to be *axially* oriented inside both CD cavities. MM and MD calculations also demonstrated the stability of the 1:1 and 1:2 stoichiometry complexes.

Keywords: cyclodextrins; self-association; fluorescence; complexation; molecular dynamics

1. Introduction

Cyclodextrins (CDs) are cyclic oligosaccharides composed of 6, 7 or 8 D-glucopyranose termed α-, β- and γ-CD respectively. Because of their hydrophobic cavity, CDs are capable of forming inclusion complexes in water with a great variety of organic compounds(*1*), which makes them ideal for many supramolecular applications (*1a, 2*). Inclusion abilities, selectivity, carrier capability and many of their properties and applications can be improved by covalently appending a substituent to the CD (*mono*CD)(*3*) or well tethering by one, or several linkers, two (*4*), three, or even more CDs (*bis*-, *tris*-, … *n-mer*-CDs) (*5*). When substituted with chromophore moiety, CD derivatives are also useful for sensing (*3a,d,h-j,l,n,o, 4a,h, 6*) and light harvesting hosts (*3b,c,e, f,k*) applications. Furthermore, the presence of this chromophore make possible to explore its structure and conformations, as well as to study self-assembling in solution and complexation with guests (*3p-v, 7*). Depending on nature of the substituent, *mono*CDs can experience self-inclusion and/or self-aggregation, as well as the functionalization can tune up complexing activity. On the other hand, it has been demonstrated that the cooperation of two CDs and the presence of the linker which provides additional binding interactions, significantly enhances molecular recognition and selectivity for guest in *b*isCDs as compared with the native or *mono*CDs. These properties are improved for *n*-merCDs which, obviously, enlarge drug-carrier and delivery capabilities by increasing drug-host ratios and binding (*5e*).

Our group has reported (*7*) the study of the complexation of dimethyl 2,6-naphthalenedicarboxylate (DMN), a fluorescent polarity sensitive probe, with *m*ono- and *bis*βCD derivatives whose appended group or linker contain the 1,3-diphenoxy moiety *i.e.*, 6[4-((3-(prop-2-ynyloxy)phenoxy)methyl]-1*H*-1,2,3-triazol-1-yl]6-deoxy-βCD (from now on, **1'**) and 1,3-bis((1-(6'deoxy-βCD-6'-yl)-1H-1,2,3-triazol-4-

yl)methoxy)benzene (from now on, **2'**). DMN does not complex with the *m*onoderivative **1'** as its self-aggregation is too strong to be displaced (*3v*). DMN, however, gives 1:1 and 2:1 stoichiometry complexes with **2'**. Association constants of DMN for each βCD cavity of **2'** in the 2:1 complex were 7 times larger than that one reported for the complexation of DMN with native βCD (*8*). The complexation of DMN with **2'** has $\Delta H^0 < 0$ which is very similar to the value obtained for DMN with native βCD, whereas $\Delta S^0 > 0$ is typical of complexes where the guest is located inside the CD cavities. Molecular Dynamics was also used to simulate the complexation processes in the presence of water. Inclusion was mostly dominated by van der Waals interactions.

The present work aims to investigate the behaviour of *mono*- and *bis*derivatives which lack chromophore groups in very diluted water solution, as well as to study the thermodynamics of their complexations with DMN. These modified βCDs are the 6^I-deoxy-6^I [4-(hept-6-ynyl)-1H-1,2,3-triazolyl]-β-cyclodextrin (**1**) and the 1,5-bis((1-(6^I-deoxy-β-cyclodextrin-6^I-yl)-1*H*-1,2,3-triazol-4-yl)methoxy) pentyl (**2**). A combination of steady-state and time-resolved fluorescence and Circular Dichroism (*ICD*) spectroscopic techniques, as well as and Molecular Mechanics (MM) and Molecular Dynamics (MD) calculations were used. Then, our interest is focused on predicting the structure and conformations of **1** and **2** in dilute aqueous solution and in the presence of DMN guest. Complex formation stabilities with DMN, stoichiometries and enthalpy and entropy changes were also investigated. The results were compared with those obtained for isolated **1'** and **2'** and in the presence of the same guest (*3v, 7*). To know how the nature of the appended groups and linker influences on **1** and **2** processes in solution and in the DMN complex stabilization is another objective. The behaviour in water and structural study of **1** and **2** complexation could also serve to further the understanding of the complexation processes with other interesting guests, such as

adducts that contain Gd(III) chelates which have applications as contrast agents (CAs) for MRI diagnosis.

2. Results and discussion

2.1. Synthesis of monoCD (1) and bisCD (2)

The Cu(I)-catalyzed Huisgen 1,3-dipolar cycloaddition was exploited for the synthesis of *mono*CD **1** and *bis*CD **2** (Scheme 1) . 6^{I}-Azido-6^{I}-deoxy-βCyD was reacted with nonadyine to afford to **1** in almost quantitative yield (*5e*). The monoCD derivative **1** was furthermore reacted with a slight excess of 6^{I}-azido-6^{I}-deoxy-βCyD with metallic copper catalysis under sonochemical conditions to obtain the product **2** in 29% yield. As already mentioned in the literature (*9*), the use of metallic copper simplify the workup procedure and avoid the formation of copper/βCD inclusion complex. All the products were isolated as solids, the chemical structures were confirmed by ^{1}H NMR, ^{13}C NMR and mass spectroscopy (see Figure 1S-3S of the Supporting Information).

2.2. Absorption and fluorescence of **1** *and* **2** *in the presence of DMN*

*Mono*CD (**1**) showed low solubility in water: above ~10^{-4} M certain turbidity begins to appear in the solution. To study the complexation with DMN, the experiments were performed by varying the **1** concentration in a narrow interval from 0 to 10^{-4} M at [DMN] ≈10^{-6} M.

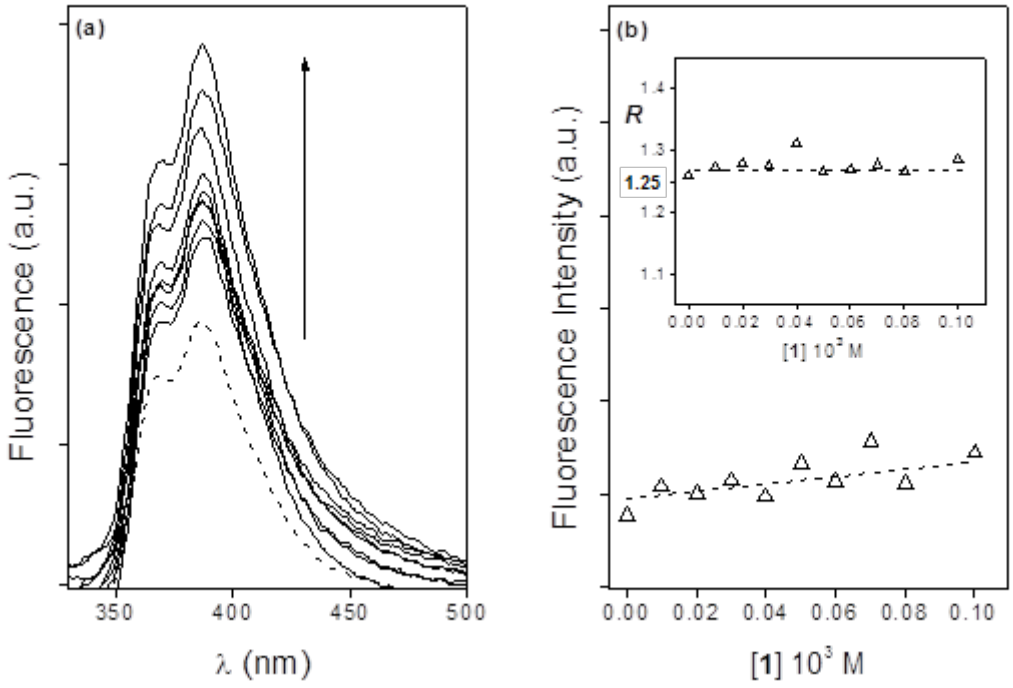

Figure 1. (a) Emission spectra of the DMN (10^{-6} M) in the absence (---) and presence of **1** at different concentrations (—); (b) Fluorescence intensity measured at 365 nm (△) as a function of [**1**]. Superimposed is the representation of *R* parameter versus [**1**] at [DMN]≈10^{-6}M. Measurements were performed at 25ºC.

The fluorescence emission spectra of the aqueous DMN solutions in the absence and presence of **1** are depicted in the left of Figure 1 and the fluorescence intensity exhibits a monotonic slight increase when increasing the [**1**], although there appears to be no displacement of any of the typical DMN bands (*7-8*). Isoemissive points that are characteristic to the existence of possible equilibria are not detected either. Monitored in Figure 1 (right), is a parameter *R* which hardly show any variation with [**1**]. *R*, obtained by the ratio of fluorescence intensities at ~389 nm and ~369 nm, is a parameter quite sensitive to changes in polarity surrounding the DMN probe and other esters naphthalene carboxylic and dicarboxylic acid derivatives (*7-8*). This would point out “a

priory" that the complexation between the DMN and the *mono*cyclodextrin derivative **1**, if it does exist, is very small.

Time resolved fluorescence measurements hardly provided any information either. The fluorescence profiles for DMN aqueous solutions at the different **1** concentrations, always adjusted to the monoexponential decays, provided lifetimes that were within the 12.6-13.3 ns interval (at 25ºC) apparently showing no significant tendency with [**1**]. These lifetimes, because of their match with that for a DMN dilute water solution in the absence of **1** at the same temperature ($\tau \approx 13$ ns), can be attributed to free DMN. No DMN complexation appears to be taking place. Nevertheless, the results should be interpreted with some caution due to the small interval of concentrations of the **1** used, which was imposed by its poor solubility.

The absorption spectrum of the isolated DMN solution (Figure 4S of the supporting information) shows bands at 295, 285 nm and at 243-245 nm, this last one a bit more intense, although they generally have little intensity due to the low chromophore concentration. The bands above 295 nm do not appear for the same reason. Absorption spectra for DMN aqueous solutions in the presence of **2** exhibit similar features, but in addition, they have a very intense band centred at ~220 nm. The intensity of this band increases significantly with [**2**] just as with those, but to a much lesser extent, that appear at 295 nm and 285 nm. **2** that absorbs around 220 nm obviously contributes to the linear increase with [**2**] that this band experiments. In general, the other absorption bands, due to the partial overlapping of the most intense 220 nm band of **2**, also grow in intensity in a linear manner.

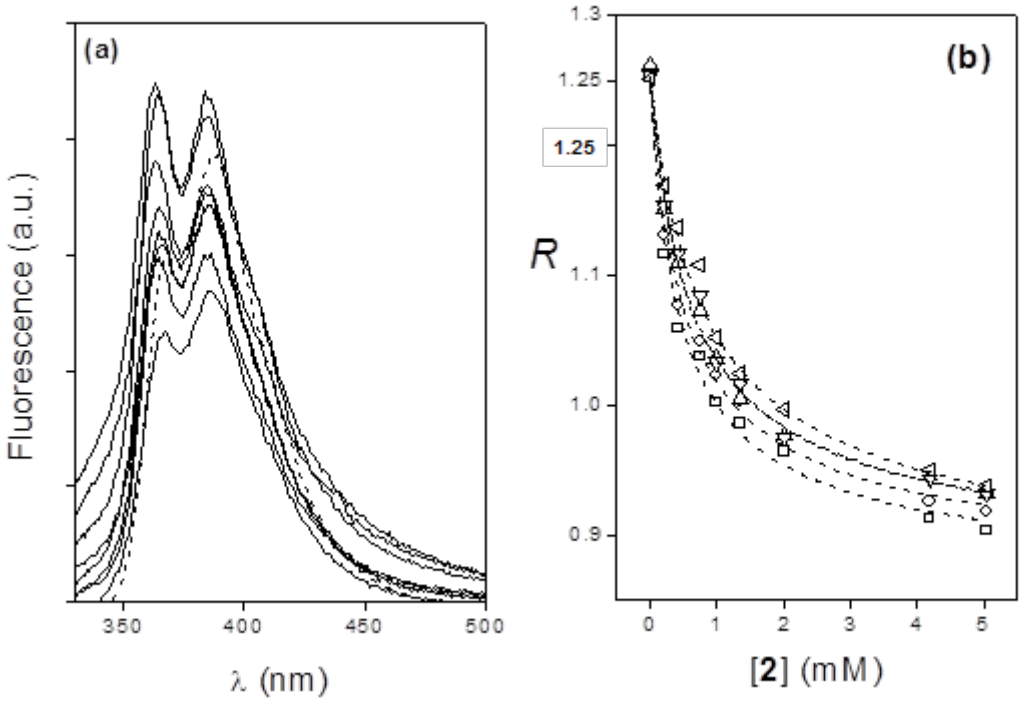

Figure 2. (a) Emission spectra of the DMN in the absence (---) and presence of different concentrations of **2** (—) at 25 ºC; λ_{exc}=295 nm; (b) Variation of parameter *R* with [**2**] at several temperatures: 5 ºC (□), 15 ºC (○), 25 ºC (△), 35 ºC (▽) and 45 ºC (◁).

Figure 2 (a) represents the emission spectra of the DMN solutions in the absence and in the presence of **2** which exhibit the two typical ~369 and ~389 nm DMN bands. The global intensity of the spectrum slightly increases with the [**2**] and slight displacement of both bands towards the blue by about 4-5 nm is also observed. Nevertheless, one of the main features, which indicates the formation of the DMN:**2** complex, is that their relative intensities significantly varies upon **2** addition at any of the temperatures. In Figure 2 (b) is depicted the variation of *R* with [**2**] at different temperatures. This variation displays a behaviour that is similar to that observed in the case of the complexation of DMN with the native βCD (*8*), **2'** (*7*), as well as of other naphthalene carboxylic and dicarboxylic esters with several CDs (*7-8, 10*). *R* in Figure 2(b) suddenly decreases until getting a [**2**] at which it reaches a nearly constant value between 0.90 and 0.95. At each individual concentration, *R* increases slightly with the temperature as a consequence of a larger fraction of the free DMN guest.

Fluorescence depolarization experiments on the same solutions were also carried out selecting 385 nm as emission wavelength. These, however, did not provide much information. The fluorescence anisotropy *r* did not exhibit a clear variation with [**2**]. In all the cases the *r* values were positive and somewhat close to zero.

In addition, fluorescence decay profiles for DMN/**2** aqueous solutions were monitored by exciting the DMN (at 295 nm) and selecting the emission at 385 nm. In all cases, two lifetime components whose contribution depends on [**2**] were obtained: (*i*) A fast component that varies from ~1.8 ns to ~4.4 ns and whose contribution increases with [**2**] until [**2**]≈2.0×10^{-3} M, to subsequently remain constant, and that slightly decreases with temperature. This component might be attributed to the DMN:**2** complex (if for the formation of the complex is exothermic, as we assume). (*ii*) A second slower component in the ~11.0-14.4 ns range which is assigned to the free DMN as its contribution diminishes with [**2**] and increases with temperature. The contribution decreasing takes place until [**2**]≈2.0×10^{-3} M to subsequently remain constant. The balance between the lifetime value for each component and their contributions to the fluorescence, produces the global decrease with [**2**] of $<\tau>$, obtained by eq. 2, shown in Figure 3.

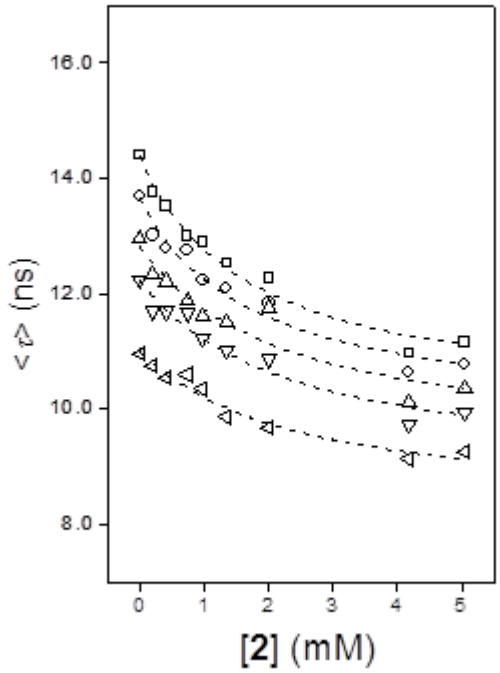

Figure 3. Variation of the $<\tau>$ with the [**2**] at different temperatures: 5 ºC (□), 15 ºC (○), 25 ºC (△), 35 ºC (▽) and 45 ºC (◁).

*2.3. Stoichiometry, association constants and enthalpy and entropy changes for the DMN:***2** *complexation*

Job's plots (*11*) were performed at several temperatures. Plots (Figure 5S of the supporting information), when *x* was calculated per mol of **2**, exhibit a maximum located at $x \approx 0.35$, which slightly displaces to ~0.4 at the lowest temperatures. This maximum, however, was placed at $x \approx 0.5$ when the molar fraction was obtained per mol of the CD cavity. These results indicate that the predominant global stoichiometry of the complex formed is close to 2:1 (DMN_2:**2**), where two molecules of DMN,

presumably located inside or close to each of the CD cavities, interact with one **2** host molecule.

From the *R* and <τ> changes with [**2**] it is possible to obtain the association constants of the global complexation process *K*, as well as the K_1 and K_2 binding constants ($K=K_1 \cdot K_2$) for the stepwise complexation process, by using the equations and protocols described in the supporting information and elsewhere (*7*). As an example, curves depicted in Figure 2(b) adjust the experimental data to the appropriate equation. Table 1 collects global association constants *K*, as well as K_1 and K_2, Φ, R_0 and R_∞ parameters at several temperatures that results from these adjustments.

TABLE 1. Values of experimental R_0 ($R_{0,exp}$) and calculated R_∞, Φ, global association constant, *K* and K_1 and K_2 binding constants ($K=K_1 \cdot K_2$) for the stepwise complexation process at different temperatures.

T (ºC)	$R_{0,exp}$	R_∞	**Φ**	$K\times10^{-8}$ (M^{-2})	$K_1\times10^{-2}$ (M^{-1})	$K_2\times10^{-6}$ (M^{-1})
5	1.25	0.80 ± 0.01	1.50 ± 0.20	4.1 ± 0.5	4.5 ± 1.0	0.9 ± 0.3
15	1.25	0.81 ± 0.01	1.43 ± 0.18	3.8 ± 0.4	4.0 ± 1.0	1.0 ± 0.3
25	1.26	0.81 ± 0.01	1.41 ± 0.19	3.6 ± 0.3	3.5 ± 0.7	1.0 ± 0.3
35	1.25	0.80 ± 0.01	1.40 ± 0.18	3.1 ± 0.3	2.8 ± 0.9	1.1 ± 0.4
45	1.25	0.80 ± 0.01	1.36 ± 0.34	2.6 ± 0.2	2.6 ± 0.4	1.0 ± 0.2

<Table 1>

$R_{0,exp}$ and R_∞ collected in Table 1, which are the *R* values for the free DMN and the totally complexed one, show values of ~1.25 and ~0.80 respectively, which hardly change with the temperature. The value of the parameter Φ is related to the ratio of the fluorescence quantum yields of the complexed DMN and the free one, indicating an increase of the fluorescence when DMN is complexed. This parameter come downs with the temperature, which could also indicate a smaller degree of complexation with an increase in temperature. The interpolation of the value of R_∞ in the calibration curve of *R vs* ε for DMN solution in different polarity media at 25°C (R=0.79036+2.94×10^{-3}ε+4.21×10^{-5}ε^2) (*8*) allow us to get the effective polarity (ε) of the medium surrounding DMN when complexed. DMN complexed with **2** provides ε≈10. This value is significantly lower than that one obtained when it complex with native βCD (ε≈45) where DMN fits inside the cavity (*8*), and even **2'** (ε≈22) (*7*). Other polarity sensitive probes of similar structure gave values for the inner βCD cavity in the 45±5 range (*12*). Here, the guest DMN when it complexes with **2**, is located in an even less polar medium than when it does with **2'**.

The last three columns of Table 1 collect *K*, K_1 and K_2 association constants. K_1 presents values that are somewhat lower than those for the DMN:*β*CD (*8*) complex and quite similar to those of the DMN:**2'** one (*7*). These constants decrease when the temperature increases. Nevertheless, K_2 show very high values, in the 10^6 order, even higher than those of the formation of the DMN_2:**2'** complex. $K_2>>K_1$ suggests that DMN_2: **2** is formed even at the lowest **2** concentrations. Obviously, the constants for the global process *K*, are around 10^8 and also a little larger than those obtained for the DMN_2:**2'** (*7*). It seems that the inclusion of a DMN inside one of the cavities, favours

the access of a second molecule into the other cavity of the *bis*βCD derivative. The behaviour with regard to the temperature on *K* would correspond to an exothermic complexation process, decreasing with temperature.

Equilibrium constants can also be obtained in a similar manner by managing, instead of parameter *R*, the changes of $<\tau>$ with [**2**] (derivation in the supporting information). Table 1S shows the results obtained from this method. The values of $<\tau>_{0,exp}$ and $<\tau>_{\infty}$, as expected, decrease when the temperature increases. The parameter Φ' which (related to Φ by eq. 12S) shows values that are smaller but close to the unit and they diminish slightly with the temperature. The equilibrium constants are of the same magnitude order to those that appear in Table 1 which also have the same behaviour with the temperature.

Assuming that **2** presents two equivalent binding sites for DMN, *ie*., DMN has equal affinity for each cavity, an apparent binding constant, $K_{app,}$ can be defined as $K^{1/2}$. At 25ºC (Table 1) K_{app} takes a value of ≈19000 M^{-1}. This constant is larger (×15) than that obtained for the 1:1 DMN:*β*CD (~1300 M^{-1}) (*8*) complex and even twice as large as that of the **2'** complex (*7*). This fact might be due to a better accommodation of the DMN guests in an environment that now is even more apolar than in the case of the **2'**. In general, *bis*CD derivatives usually posses better affinities for guests than their respective *mono*derivative or native CDs (*4d,e,i,l,m,s,z*).

From the association constants at different temperatures by using linear van't Hoff representations (Figure 8S of the supporting information) ΔH^0=–8±1 $kJmol^{-1}$ and ΔS^0=+137±4 $JK^{-1}mol^{-1}$ for the DMN complexation with **2** were obtained. As occurred for the DMN complexation with **2'** (*7*), the global 2:1 process has enthalpy and entropy changes that are negative and positive respectively. Likewise negative and positive

changes were obtained for DMN complexation with the native βCD *(8)* (Table 2S of the supporting information). Negative ΔH^0 values for the DMN complexation with **2**, as occurred for **2' (**and native βCD) are related to the presence of favourable attractive, probably van der Waals host-guest interactions. The process is also accompanied by an entropy change that is also very favourable, even more than in the case of **2' (**and obviously more than for βCD). This large positive entropic change in comparison to the one obtained for the 1:1 complexation with βCD, is due to the fact that the increase in disorder due to the release of ordered water molecules from two interior CDs, from the sphere that surrounds the DMN hosts, but also, to the partial desolvation of the bridge between CDs overcome the loss of degrees of freedom that the inclusion of two DMNs presents when they enter into the apolar cavities. The small differences between the complexation processes of both **2** and **2'** derivatives are clearly due to the different nature of the bridge.

2.4. Quenching experiments

Stern-Volmer representations from quenching experiments by steady-state or lifetime measurements for the isolated DMN or in the presence of native βCD, **1** or **2** by using diacetyl as dynamics quencher (Figure 9S of the supporting information) are linear in whole range of concentrations. At the concentrations of βCD and **2** used in the experiments the fraction of complexed DMN were ~79% and ~14% respectively. As stated earlier, in the concentration interval limited by its solubility, the DMN hardly complexes with **1**.

TABLE 2. Bimolecular quenching parameters of the DMN in the presence of **1**, native *β*CD and **2** from the steady-state (a) or fluorescence lifetime measurements (b).

System	$K_{S\text{-}V}$ (M^{-1})	$\langle\tau\rangle$ (ns)	$k_q \times 10^{-9}$ ($M^{-1}s^{-1}$)
DMN	54.4 ± 1.8[a]	14.5	3.7 ± 0.1[a]
	33.5 ± 1.4[b]		2.3 ± 0.1[b]
*mono*βCD:DMN	39.7 ± 0.6[a]	12.7	3.1 ± 0.1[a]
	27.85 ± 1.1[b]		2.2 ± 0.1[b]
*β*CD:DMN	34.6 ± 0.9[a]	15.9	2.2 ± 0.1[a]
	9.1 ± 0.8[b]		0.6 ± 0.1[b]
*bis*βCD:DMN_2	23.1 ± 2.4[a]	13.5	1.7± 0.2[a]
	13.3 ± 0.9[b]		1.0 ± 0.1[b]

Decay fluorescence intensity profiles for the DMN/**1** system adjusts to a single lifetime component which was similar to that obtained in the case of the isolate DMN, whereas in the presence of βCD or **2**, as stated earlier in this paper, two components came out. Nevertheless, the behaviour of both with the quencher concentration was different. Whereas the lifetime for the slower component decreases with the quencher concentration, that one for the faster one practically remains constant. On the other hand, their contributions decrease and increase respectively with the quencher concentration. This different behaviour corroborates the fact that there are two types of chromophores in solution. One of them ascribed to the free DMN, whose fluorescence is quenched rather easily, decreasing the lifetime and its contribution with quencher concentration; the other one whose lifetime remains almost constant while its relative contribution slightly increases, which is ascribed to de complexed form.

Values of k_q for the free DMN or in the presence of **1**, collected in Table 2, are relatively high and very similar, indicating that there is no or little interaction between the DMN and **1** (at the concentrations studied), so that the complexation, if it exists, will be accompanied by quite a low association constant. On the other hand, the values of k_q for DMN in the presence of βCD or **2** are much lower than the previous ones. This means that the complexation exists and that the DMN is located in an environment that is more protected against quencher. Similar conclusions were reached from both, steady state or lifetime measurements.

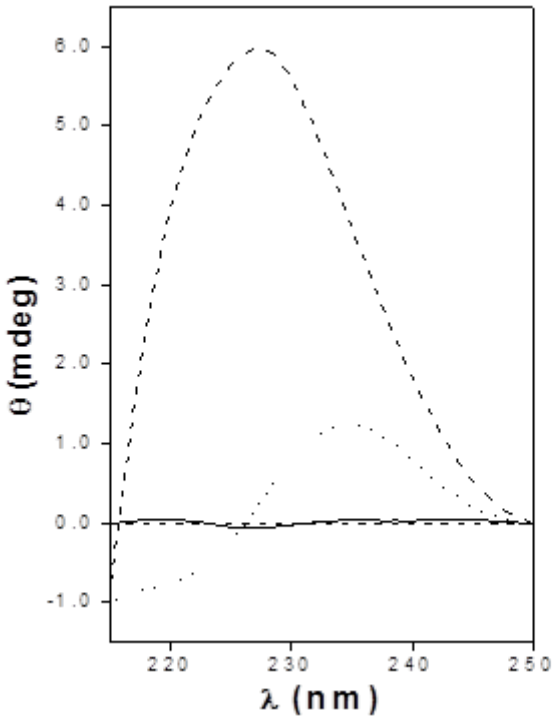

Figure 4. DCI spectra in the 215-250 nm range for DMN aqueous solution at saturation (~10^{-6}M) in the absence (—) and in the presence (---) of [**2**]=20×10^{-6} M and of [**1**]=0.1×10^{-3} M (····) carried out with cells of 10 cm and 1 cm respectively a 25 ºC.

2.5. Circular Dichroism Spectra

Figure 4 collects the Circular Dichroism spectra for DMN in the absence and in the presence of **2** for the region where the most intense DMN transition (^1B_b), whose moment is oriented along the long naphthalene ring axis, takes place (*3s*, *13*). In the absence of a **2**, the DMN solution shows no dichroic signal due to its achirality, whereas in its presence, an induced positive band centered ~230 nm can be observed as a consequence of the complexation. In addition, this positive sign (*3s*, *13-14*) would indicate that the DMN might be *axially* included into the CD cavities of **2**. These results are similar to those obtained by Harata and col. (*15*) for the complexation of naphtalene monosubstituted (in β position) derivatives with native βCDs. In the case of the DMN/**1**, the low DCI signal only indicates that the DMN if it interacts only does so slightly.

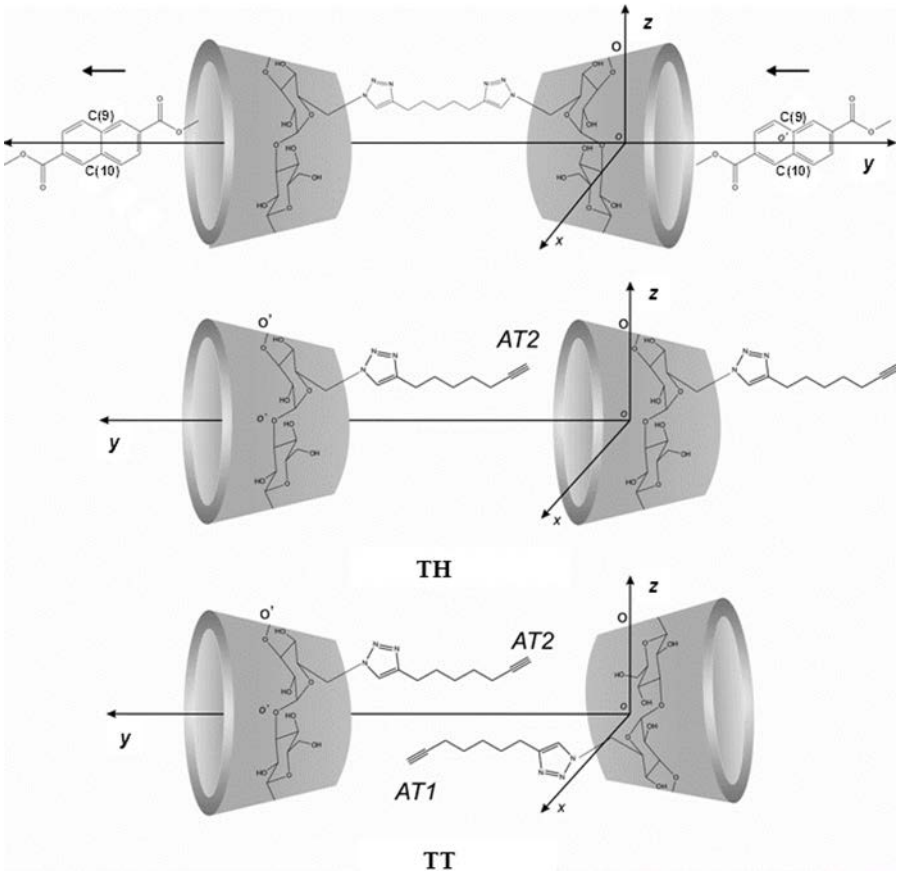

Figure 5. Different approaches carried out for the structures of the possible complexes of the **2** with DMN (upper), as well as of the non-covalent $(\mathbf{1})_2$ dimers (lower). *O* represents a bridging oxygen atom located on the coordinate axis *z* of the first *mono*derivative and *O'* another bridging oxygen atom located in the second one. The atoms AT1 or AT2 correspond to the carbon terminal of the appended group of CD1 and CD2 respectively.

2.6. Theoretical simulations of the non-covalent **1** *dimers*

2 ns MD simulations were performed on the optimized tail-head (TH) and tail-tail (TT) arrangements for the non-covalent dimers of **1** *mono*derivative in aqueous solution depicted in Figure 5, according protocols described later in this manuscript (*3v*). Initial minimized structures are depicted in Figure 10S of the supporting information.

The histories of the distances between the centers of mass of the two CD macrorings, of each **1** derivative cyclodextrin, CD1 (or CD2) and the terminal C(sp) atom, AT2 (or AT1) of the appended group of the partner derivative, as well as the total binding energies between **1** derivatives obtained from the analysis of the 2 ns MD trajectories the solvated TT and TH arrangements are depicted in Figure 6.

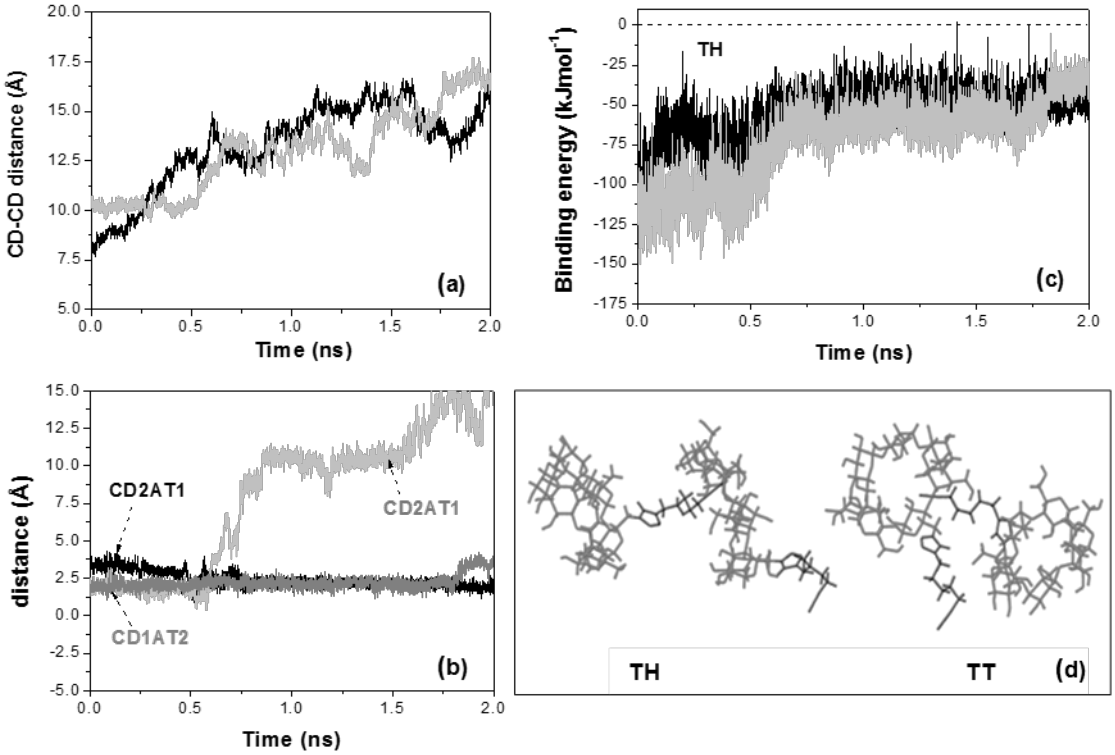

Figure 6. Histories of the (a) CD-CD; (b) CD2-AT1 and CD1-AT2 distances and of the (c) binding energies obtained from the analysis of the MD trajectories on the minimized, TH (dark) and TT (grays). (d) Structures of the TH and TT $(\mathbf{1})_2$ dimers at the end of the 2 ns trajectories. The AT corresponds to the end-carbon atom of the appended group.

Even though the CD-AT distances corresponding to the TH arrangement indicate that the appended group remains close to the CD cavity during the trajectory, as well as one of the substituent groups for the TT, (the other one leaves the cavity at the first quarter of the trajectory), the value of the distance between CDs indicates that the two *mono*derivatives split up with time. This means that the binding energies become less favourable and apparently the dimer dissociate with time. This did not occurred with **1'** dimers (*3v*), where the presence of a phenoxy moiety in the appended group makes both arrangements remain stable with time. Figure 6 also displays the resulting TH and TT

structures at the end of the trajectory. Some geometrical parameters and binding energies related to the MD are collected in Table 3S (supporting information). The $(\mathbf{1})_2$ dimers seem to be quite unstable meaning that the fraction of the free **1** in water solution capable of complexing with DMN should be quite high. In spite of this all experimental evidences shown the almost lack of DMN complexation with **1.** On the contrary, the absence of DMN complexation with **1'** was, however, attributed to the large $(\mathbf{1'})_2$ dimers stabilities. The complexation with DMN was not able to compete with dimerization (*3v*,*7*).

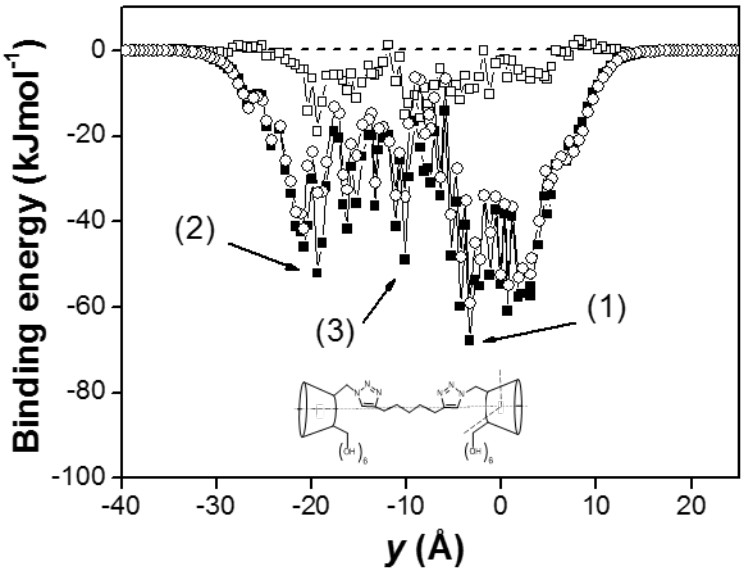

Figure 7. Variation of the total binding energy (■), electrostatics contribution (□) and that of van der Waals (○) during the approaching of the DMN host to **2** along the *y* axis (Å).

2.7. Theoretical simulations of the complexation of 2 *with* DMN

MM calculations, as stated before, were carried out using the totally extended conformation of 2 as a starting structures. The results, which are summarized in Figure

7, show two local minima binding energy (BME) arrangements located at y_1 = –3.3 Å (E_{MBE} = –67.9 kJmol^{-1}) and y_2 = –19.4 Å (E_{MBE} = –52.1.9 kJmol^{-1}) where the DMN is placed inside each of the CD cavities. Nevertheless, located between the two cavities at y_2 = –10.1 Å (E_{MBE} = –49.0 kJmol^{-1}) another less significant local MBE structure, is also observed. The electrostatic contributions to binding energies were less important than van der Waals ones. These contributions were –18.9 and –33.2 kJmol^{-1}, –2.7 y –73.8 kJmol^{-1} and –15.0 and –34.1 kJmol^{-1} respectively.

The MBE structures in which the DMN is placed inside one or two of the CD cavities (1 and 2) and that in which it is between both cavities (3) were used to build the initial arrangements of the 1:1 and 2:1 stoichiometry DMN:**2** complexes which, minimized again, served as the basis to carry out the MD simulations following the protocols described later in this manuscript. The 1:1 stoichiometry complexes, (DMN:**2**)$_{in}$ and (DMN:**2**)$_{out}$ were built by placing the host DMN in the positions (1) or (3), inside and outside the cavity, respectively. For the 2:1 complex, DMN$_2$:**2**, both host molecules were placed in the positions of (1) and (2), inside both cavities, as is shown in Figure 7.

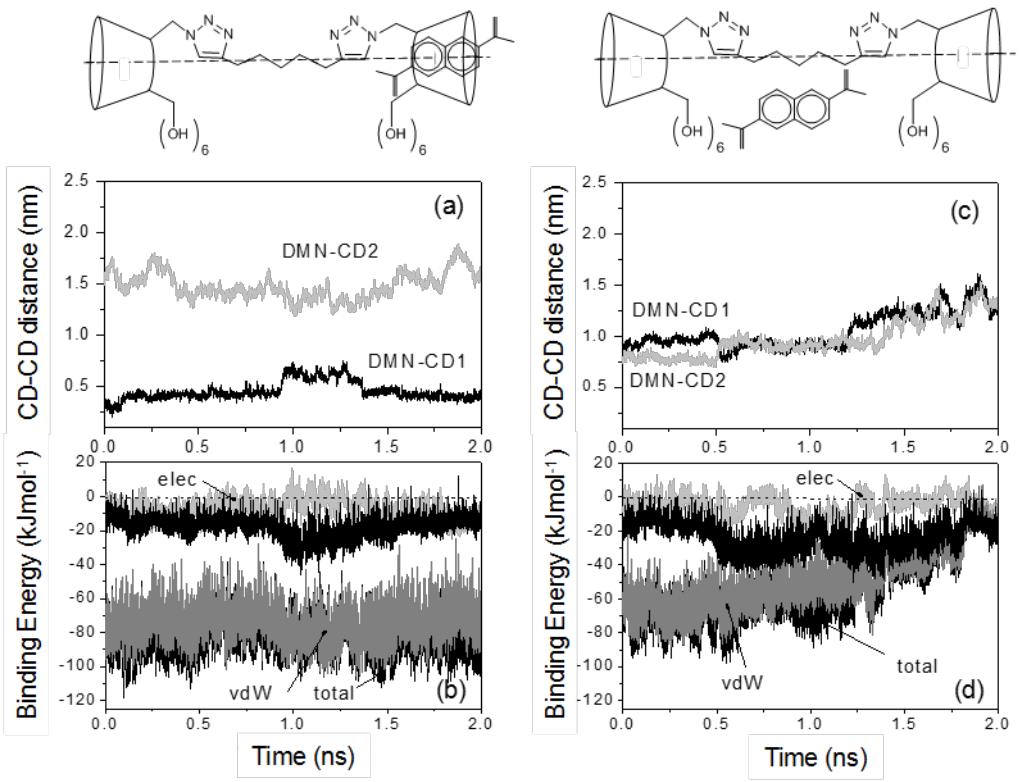

Figure 8. Histories of the CD1-DMN (—) and CD2-DMN (—) (a,c) distances and of the total binding energies (black), van der Waals (dark gray) and electrostatics (gray) contributions and DMN-spacer interaction (black) (b,c) for the 1:1 stoichiometry (DMN:**2**)$_{in}$ (left) y (DMN:**2**)$_{out}$ (right) structures drawn above.

The histories of the distances between the DMN and the centre of mass of CD cavities for the 1:1 (DMN:**2**)$_{in}$ complex, which are shown in Figure 8 (a), indicate that the DMN does not remain completely inside the CD cavity during the trajectory. The average of the DMN-CD1 distances is 4.6 ± 0.9 Å, which means that a large portion of it is placed outside the CD by the side of the linker. Table 4S of the supporting information collects the averages of some of these geometric, as well as energetic parameters. Figure 8 (b) also shows the variation of the interaction energies with time between the DMN guest and **2** and the linker. It is remarkable that the 1:1 (DMN:**2**)$_{in}$ complex is stable

throughout the trajectory. Most of the stabilization of the systems comes from van der Waals interactions. Figure 9 (top) depicts the MBE structure for the 1:1 (DMN:**2**)$_{in}$ complex.

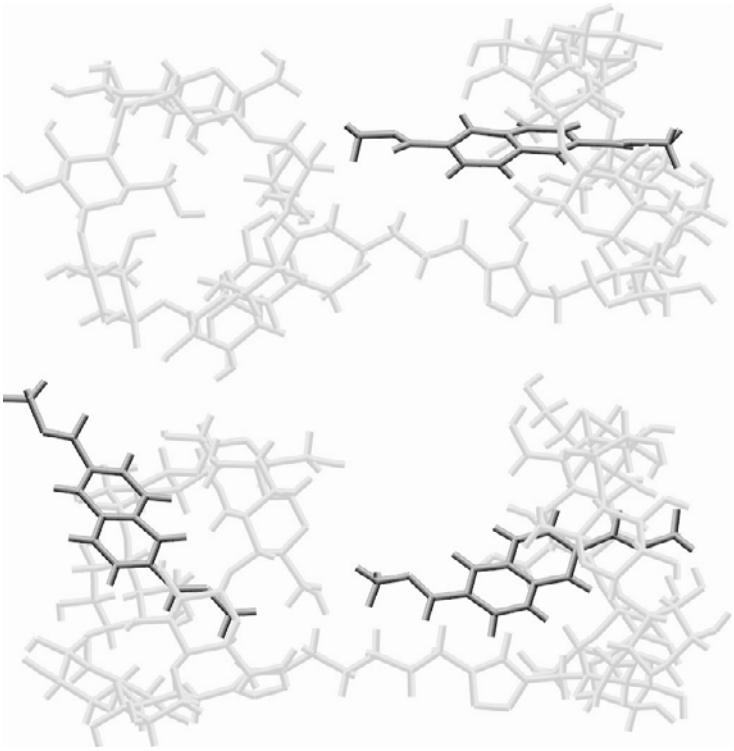

Figure 9. MBE structures obtained from the analysis of the 2 ns MD simulations carried out on (DMN:**2**)$_{in}$ (upper) and DMN_2:**2** (lower) systems respectively. Some of the geometric and energetic parameters that are characteristic of these structures are collected in Table 4S.

Looking at the histories for the 1:1 (DMN:**2**)$_{out}$ complex depicted in Figure 8 (c,d) the CD-DMN distances increase while the binding energies decrease with time. Although these energies seem initially remain quite favourable due to the fact that the DMN accommodates between both CDs with the ester groups partially into the cavities by the primary faces, this arrangement is not stable with time. In fact, an additional 2 ns simulation shows how the complex completely dissociates during the third nanosecond of the trajectory.

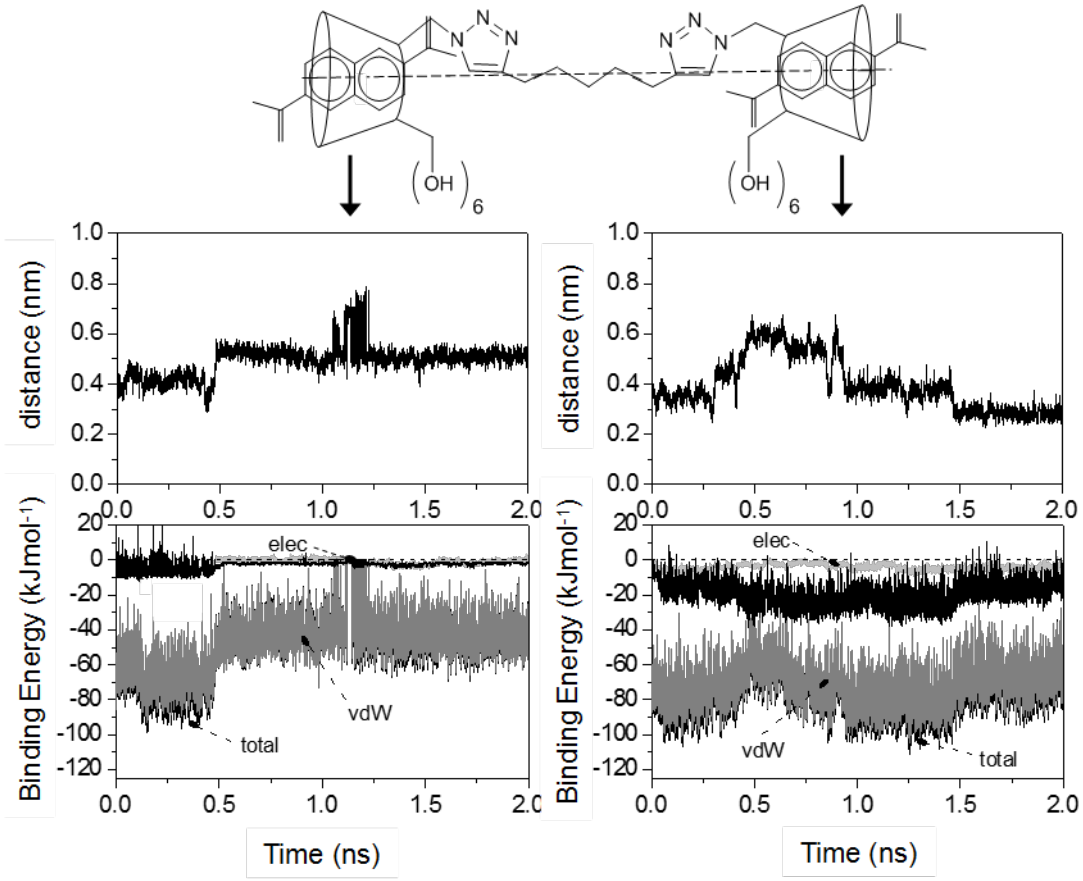

Figure 10. History of the distances between each DMN and the center of mass of its corresponding βCD cavity (—) (top panel). Binding energies between each DMN and **2** (black), van der Waals (gray), electrostatics (dark gray) and DMN-linker interaction contributions that join both CDs (black) (lower part) in the DMN_2:**2** complex of 2:1 stoichiometry.

Figure 10 depicts the results of the analysis of the simulations for the 2:1, DMN_2:**2** complex. The averages of some geometrical and energetic parameters and the minimum binding energy are collected in Table 4S of the supporting information. These results indicate that the DMNs, even though they do not remain completely within their corresponding cavities throughout the dynamics, they do close to them. In fact, one of the DMN in CD1 (1) penetrates into the cavity partially slightly leaving from the linker side,

whereas the other one, in CD2 (2), does so by the opposite side. As a consequence, the DMN-linker interaction energies are larger in (1) than in (2), as can be observed in Figure 10 and in the collected average values of Table 4S. Total binding energies and contributions are also depicted in Figure 10. The binding energies DMN-**2** are favourable in both cases, van der Waals attractive interactions being the main contribution to them. If we compare them with those obtained for the DMN_2:**2'** system (*7*), due to the fact that the DMNs are partially located inside the cavity, they are now slightly less favourable. Figure 10 (bottom) represents the MBE structure for the 2:1 DMN_2:**2** complex, showing the location of each DMN with regard to the CD cavities which is partially outside them.

3. Conclusions

The modified **1** and **2** *mono*- and *bis*CD derivatives studied are characterized by the absence of chromophore groups and, especially the **1**, for its low solubility in water. For this reason its behaviour in aqueous solution was predicted by MD simulations. Nevertheless, the complexation of DMN with **1** and **2** was followed by fluorescence techniques, circular dichroism measurements and Molecular Mechanics and Dynamics simulations.

DMN interacts weakly with monoCD **1**, at least in the limited concentration interval studied. Even though the fluorescence intensity of the DMN/**1** solutions slightly increases with the [**1**], the parameter *R*, the fluorescence lifetime and the bimolecular quenching constant hardly change. They were very similar to those obtained for isolated DMN aqueous solutions. Nevertheless, the slight DCI signal also points to a potential weak DMN–**1** interaction.

On the contrary, the DMN does appear to form stable complexes with **2**. The 2:1 (DMN:**2**) stoichiometry is predominant. Both global complexation process *K* association constants, as well as those, K_1 and K_2 for the stepwise complexation process were obtained. The association constants of the first equilibrium present relatively low values that decrease with temperature (like the global constants), whereas that of the second show much higher values. In addition, the cooperating binding behaviour of both cavities in **2** favours the formation of the complex if compared to the native βCD cavity. The global complexation process presents a negative enthalpy change, the entropic term, however, is the one that favours and governs the process. The DMN bimolecular quenching experiments indicate that the efficiency of DMN quenching is much larger in the absence than in the presence of native βCD and **2**. The DCI spectrum shows that the DMN appears to be included partially inside the **2** cavities *axially* oriented. The medium that surrounds the DMN complexed with the **2** is quite apolar (ε~10), even more apolar than that obtained with the **2'**.(*7*)

The Molecular Dynamics simulations support the fact that the **1** could form non-covalent TH dimers. Nevertheless, their stability is much less than that of the $(\mathbf{1}')_2$ dimer (*7*). However, the simulations show that the DMN can form stable complexes with **2** of 1:1 and 1:2 stoichiometries.

4. Experimental

4.1. Synthesis, Reagents, and Solutions.

Mono- and *bis*derivatives of β-cyclodextrin, 6^I-deoxy-6^I [4-(hept-6-ynyl)-1H-1,2,3-triazolyl] β-CD (*mono*CD, **1**) and 1,5-bis((1-(6^I-deoxy-β-cyclodextrin-6^I-yl)-1*H*-1,2,3-

triazol-4-yl)methoxy) pentyl (*bis*βCD, **2**) studied and depicted in Scheme 1, were synthesized as follow:

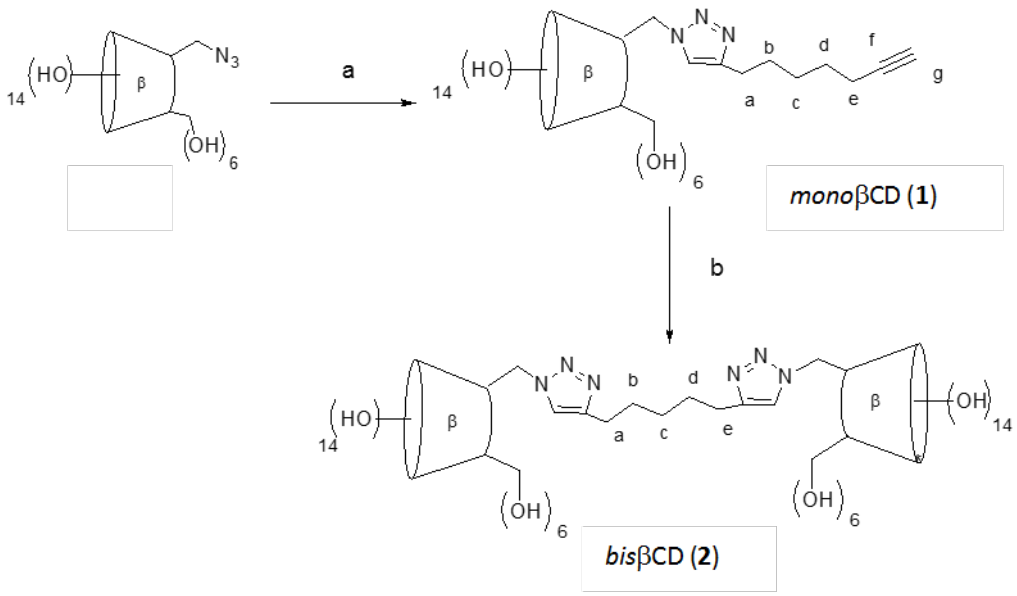

Scheme 1. Synthesis of β-CD alkyniltriazolyl derivative *mono*CD, and of the symmetric dimer *bis*CD. *Reagents and conditions*: a) 1,8-nonadiyne, $CuSO_4 \cdot 5H_2O$, *L*-ascorbic acid, DMF, MW,70°C b) Cu powder, MW/US, 85 °C, 2h.

***4.1.1. Synthesis of 6^I-deoxy-6^I [4-(hept-6-ynyl)-1H-1,2,3-triazolyl] β-CD* (1).** The product was synthesized as described in the literature (*5e*).

***4.1.2. Synthesis of symmetric β,β CD dimer,* (2).** The reaction was carried out in a 50 mL heavy walled pear-shaped three-neck flask with non-standard taper outer joint. The fine turnings of metallic copper (21 mg) were suspended in 5 mL of DMF, 47 mg of 6^I-deoxy-6^I [4-(hept-6-ynyl)-1H-1,2,3-triazolyl] β-CD (**1**) (0.036mmol) and 63,8 mg of 6^I-azido-6^I-deoxy-β-CD, (0.055 mmol) were added, and the mixture was irradiated with MW/US for 2 h at 100°C (US 20 KHz, MW max power 70 W). The copper was filtered off on paper filter and washed with water. After evaporation of the solvent under vacuum, the crude product was purified by flash-chromatography on RP18 with a

gradient from water to methanol, affording 26 mg of pure compound *bis*CD (0.0106 mmol, 29%). *Bis*CD is a white powder; R_f = 0.14 (iPrOH/H_2O/AcOEt/NH_4OH 5:3:1:1); νmax (KBr)/cm^{-1} 3422, 2931, 1463, 1371, 1042, 1030, and 761; ^1H NMR (300 MHz; DMSO-d_6): 7.8 (s, 2H, H-4 triazole), 5.91-5.69 (m, 28H, O(2)H, O(3)H), 5.08 (m, 2H, H-1'), 4.88-4.78 (m, 14H, H-1, H-6'^{A}), 4.6-4.54 (m, 14H, O(6)H, H-6'^{B}), 4.38 (m, 2H, H-5), 4.013 (m, 2H, H-5'), 3.9-3.1 (m, overlaps with H_2O, H-6, H-3, H-2, H-4, H-5), 2.97 (m, 2H, H-6) 2.62 (m, overlaps with DMSO, H-e, H-a), 1.68 (m, 4H, H-b, H-d), 1.48 (m, 2H, H-c); ^{13}C NMR (75 MHz; DMSO-d_6): 147.88(C-4 triazole), 124.16 (C-5 triazole), 103.122 (C-1), 102.24 (C1'), 84.51, 84.55, 82.56, 81.8 (C4), 74.11, 73.4, 73.16 (C-2,C-3,C-5), 71.07 (C-5'), 61.001, 59.72 (C6), 51.67 (C-6'), 29.78 (C-b, C-d, C-c)26.02 (C-a, C-e); m/z (ESI) calcd. for $C_{93}H_{150}N_6O_{68}$ 1220.42 $[M+2H]^{2+}$, 1231.42 $[M+Na+H]^{2+}$, 1242.42 $[M+2Na]^{2+}$, found 1241.7 $[M+2Na]^{2+}$, 1231.66 $[M+Na+H]^{2+}$, 1220.68 $[M+2H]^{2+}$ (Figure 1S-3S of the supporting information).

Dimethyl 2,6-naphthalenedicarboxylate (DMN), purchased from Aldrich, was recrystallized from methanol. Aqueous (MilliQ) DMN/*mono*- and *bis*βCDs solutions were prepared by weight using an aqueous filtered (0.2 μm ∅, PTFE, Advantec) DMN saturated solution (10^{-6} M) that was held constant in all experiments. DMN/*m*βCD (DMN/*b*βCD) solutions in the 0-2.77×10^{-4} M (0-5.11×10^{-3} M) range were stirred for at least 36 h prior to measuring.

4.2. Instrumentation

Absorption spectra were recorded using a Perkin-Elmer Lambda-35 spectrometer. Steady-state fluorescence and time-resolved measurements were performed in SLM 8100 AMINCO and TCSPC FL900 Edinburgh Int. spectrofluorometers. Characteristics and measurement conditions have been previously described (*3r,v, 7, 16*). The

excitation for fluorescence lifetime measurements was carried out using a pulsed NanoLED (IBH) emitting at 295 nm. Data acquisition was carried out using 1024 channels with a time window width of 125 or 200 ns and a maximum total of 10,000 counts at the peak of intensity decay function. Decay intensity profiles were fitted to a sum of exponential decay functions by the iterative reconvolution method as (*17*):

$$I(t) = \sum_{i=1}^{n} A_i e^{-t/\tau_i} \qquad (1)$$

And the intensity weighted average lifetime of a multiple-exponential decay function was then defined as (*18*):

$$\langle \tau \rangle = \frac{\sum_{i=1}^{n} A_i \tau_i^2}{\sum_{i=1}^{n} A_i \tau_i} \qquad (2)$$

where A_i is the pre-exponential factor of the lifetime component τ_i.

Samples in both instruments were temperature controlled by two Huber Ministat baths. Squared 10mm path conventional quartz cells, right angle geometry were used. Polarizers were placed at and magic angle conditions except for depolarization measurements. The fluorescence anisotropy *r* is defined as (*19*):

$$r = \left(I_{VV} - G\, I_{VH}\right) / \left(I_{VV} + 2G\, I_{VH}\right) \qquad (3)$$

where I_{xy} is the emission intensity that is measured when the excitation polarizer is in position x (V for vertical, H for horizontal), the emission polarizer is in position y, and the *G* factor (= I_{HV}/I_{HH}) corrects for any depolarization produced by the optical system.

For a single excited species which is dynamically quenched with Q, the ratio of fluorescence intensity, in the absence of Q and in its presence, are related to [Q] by the

Stern-Volmer equation. The slope of Stern-Volmer plots in the linear region provides the quenching constant K_{SV}, which is also related to a bimolecular quenching constant k_q (*20*).

Induced Circular Dichroism (*ICD*) spectra were recorded in a JASCO J-715 spectropolarimeter. Recorded spectra were the average of 3 scans taken at the speed of 20 nm/min with a time response of 0.125 s. Bandwidths were set at 2 nm and the sensitivity and resolution at 20 mdeg and 0.5 nm respectively. Measurements were performed at 25ºC in 10 cm and 10 mm optical path cells.

4.3. Theoretical Methods

Calculations were performed in the presence of water using SybylX-2.0 (*21*), and the Tripos Force field (*22*). A relative permittivity value of ε = 1 was used. Partial atomic charges were calculated using the semi-empirical program MOPAC and a AM1 Hamiltonian (*23*). Charges for the CD macroring and for the appended group and linker (in the all *trans* conformation) were obtained separately. Charged for DMN were those used previously (*8*). Non-bonded cut-off distances were set at 8 Å. Optimisation was carried out using the MAXIMIN2 algorithm and the conjugate gradient was used as the termination method (*24*). Periodic boundary conditions (PBC) and the silverware algorithm were used for water solvation (*25*).

4.3.1. Protocols for the formation of 1:1 and 2:1 stoichiometry complexes. For the DMN complexation with **2**, this was placed in the optimised, most extended, conformation in vacuum in such a way that the glycosidic oxygen centre of mass of one CD was located at the origin of the coordinate system (*o*) with the y axis oriented along the main CD axis and the z axis passing through a glycosidic oxygen as depicted in the top of Figure 6. The *oo'* distance projected onto the *y* coordinate (*o'* corresponds to the

centre of mass of the DMN naphthalene), the angle between the yz and the naphthalene planes (θ) and the *oo' C9* angle (δ) were used to define the relative DMN-CD orientation. Critical analysis of the binding energy for the optimised structures (gradient 0.2 kcal/molÅ), obtained by scanning δ (90 to 30º at 20º intervals), θ (-180º to 180º at 10º intervals) and *y* (in the 10 to -5 Å range at 1 Å steps) parameters *in vacuo*, provided better orientation for the approach. With δ and θ fixed, DMN was forced to pass through both CD cavities from *y* = +25 (Å) up to -40 (Å) at 0.5 Å steps along the *y* coordinate. Each structure generated was solvated (PBC), optimised (gradient 3.0 kcal/molÅ) and analysed.

The newly optimised (0.5 kcal/molÅ) DMN**:2** and DMN_2:**2** solvated minima binding energy structures (MBE) were used as starting conformations for the 2 ns MD simulations at 300K in the presence of water. MD characteristics were similar to those used previously (*7*) (i.e., equilibration period of 25,000 fs, integration time step of 2 fs, velocities rescaled at 100 fs intervals). Bonds containing H atoms were forced to not vibrate throughout the whole trajectory which consists of 8,000 images, as data were saved every 250 fs.

4.3.2. Non-covalent* 1 *dimers MD simulations. The tail-to-head (TH) and tail-to-tail (TT) arrangements for $(\mathbf{1})_2$ dimers represented in Figure 6 were used, once minimised (0.5 kcal/molÅ) as starting conformations for 2ns MD. In these two structures, well the appended group of one CD enters its CD partner via the secondary face (TH), or well the substituent of each CD mutually penetrates its neighbouring CD via the primary face (TT). Protocol were similar to those described in the previous paragraph and earlier (*3v*).

Acknowledgements

FM and TC acknowledge the assistance of M.L. Heijnen in the preparation of the manuscript.

Funding

This work was supported by the University of Turin (fondi ricerca locale 2013, ex-60%) and the Universidad de Alcalá (GC2011-002 and UAH2011/EXP-036). TC acknowledges FPI predoctoral fellowship from Spanish MICINN.

Supporting Information

NMR spectra for compounds characterization, binding constant equations derivation and supplemental figures and tables related to this article are available online.

References

(1) (a) Dodziuk, H.; Editor, *Cyclodextrins and Their Complexes*; Wiley-VCH Verlag GmbH & Co. KGaA: 2008; (b) Douhal, A., *Cyclodextrins Materials Photochemistry, Photophysics and Photobiology* Elsevier: Amsterdam, 2006.

(2) Li, S.; Purdy, W.C., *Chem. Rev.* **1992,** *92*, 1457-1470.

(3) (a) Ueno, A.; Minato, S.; Suzuki, I.; Fukushima, M.; Ohkubo, M.; Osa, T.; Hamada, F.; Murai, K., *Chem. Lett.* **1990,** *19*, (4), 605-608; (b) Berberan-Santos, M.N.; Canceill, J.; Brochon, J.C.; Jullien, L.; Lehn, J.M.; Pouget, J.; Tauc, P.; Valeur, B., *J. Am. Chem. Soc.* **1992,** *114*, 6427-6436; (c) Berberan-Santos, M.N.; Pouget, J.; Valeur, B.; Canceill, J.; Jullien, L.; Lehn, J.M., *J. Phys. Chem.* **1993,** *97*, (44), 11376-11379; (d) Hamasaki, K.; Ikeda, H.; Nakamura, A.; Ueno, A.; Toda, F.; Suzuki, I.; Osa, T., *J. Am. Chem. Soc.* **1993,** *115*, (12), 5035-5040; (e) Gravett, D.M.; Guillet, J.E., *J. Am. Chem. Soc.* **1993,** *115*, (14), 5970-5974; (f) Jullien, L.; Canceill, J.; Valeur, B.; Bardez, E.; Lehn, J.-M., *Angew. Chem., Int. Ed.* **1994,** *106*, (23/24), 2582-2584; (g) Wang, Y.; Ikeda, T.; Ikeda, H.; Ueno, A.; Toda, F., *Bull. Chem. Soc. Jpn.* **1994,** *67*, (6), 1598-1607; (h) Ikeda, H.; Nakamura, M.; Ise, N.; Oguma, N.; Nakamura, A.; Ikeda, T.; Toda, F.; Ueno, A., *J. Am. Chem. Soc.* **1996,** *118*, (45), 10980-10988; (i) Ikeda, H.; Nakamura, M.; Ise, N.; Toda, F.; Ueno, A., *J. Org. Chem.* **1997,** *62*, (5), 1411-1418; (j) Ikunaga, T.; Ikeda, H.; Ueno, A., *Chem.-Eur. J.* **1999,** *5*, (9), 2698-2704; (k) Berberan-Santos, M.N.; Choppinet, P.; Fedorov, A.; Jullien, L.; Valeur, B., *J. Am. Chem. Soc.* **1999,** *121*, (11), 2526-2533; (l) Aoyagi, T.; Ikeda, H.; Ueno, A., *Bull. Chem. Soc. Jpn.* **2001,** *74*, (1), 157-164; (m) Park, J.W.; Song, H.E.; Lee, S.Y., *J. Phys. Chem. B* **2002,** *106*, (29), 7186-7192; (n) Park, J.W.; Lee, S.Y.; Kim, S.M., *J. Photochem. Photobiol., A* **2005,** *173*, (3), 271-278; (o) Ikeda, H.; Murayama, T.; Ueno, A., *Org. Biomol. Chem.* **2005,** *3*, (23), 4262-4267; (p) Balbuena, P.; Lesur, D.; Alvarez, M.J.G.; Mendicuti, F.; Mellet, C.O.; Fernandez, J.M.G., *Chem. Commun.* **2007**, (31), 3270-3272; (q) González-Álvarez, M.J.; Balbuena, P.; Ortiz Mellet, C.; García Fernández, J.M.; Mendicuti, F., *J. Phys. Chem. B* **2008,** *112*, (44), 13717-13729; (r) González-Álvarez, M.J.; Vicente, J.; Ortiz Mellet, C.; J. M. Fernández García, J.M.; Mendicuti, F., *J. Fluoresc.* **2009,** *19*, (975-988), 975; (s) González-Álvarez, M.J.; Benito, J.M.; García Fernández, J.M.; Ortiz Mellet, C.; Mendicuti, F., *J. Phys. Chem. B* **2013,** *117*, (18), 5472-5485; (t) González-Álvarez, M.J.; Mayordomo, N.; Gallego-Yerga, L.; Mellet, C.O.; Mendicuti, F.,

Tetrahedron **2012,** *68*, (14), 2961-2972; (u) González-Álvarez, M.J.; Méndez-Ardoy, A.; Benito, J.M.; García Fernández, J.M.; Mendicuti, F., *J. Photochem. Photobiol., A* **2011,** *223*, (1), 25−36; (v) Carmona, T.; Gonzalez-Alvarez, M.J.; Mendicuti, F.; Tagliapietra, S.; Martina, K.; Cravotto, G., *J. Phys. Chem. C* **2010,** *114*, (51), 22431-22440.

(4) (a) Liu, Y.; Chen, Y.; Li, B.; Wada, T.; Inoue, Y., *Chem.-Eur. J.* **2001,** *7*, (12), 2528-2535; (b) Liu, Y.; You, C.C.; Li, B., *Chem.-Eur. J.* **2001,** *7*, (6), 1281-1288; (c) Liu, Y.; Chen, Y.; Li, L.; Zhang, H.-Y.; Liu, S.-X.; Guan, X.-D., *J. Org. Chem.* **2001,** *66*, (25), 8518-8527; (d) Liu, Y.; Li, L.; Zhang, H.-Y.; Song, Y., *J. Org. Chem.* **2003,** *68*, (2), 527-536; (e) Liu, Y.; Song, Y.; Wang, H.; Zhang, H.-Y.; Wada, T.; Inoue, Y., *J. Org. Chem.* **2003,** *68*, (9), 3687-3690; (f) Liu, Y.; Wang, H.; Liang, P.; Zhang, H.-Y., *Angew. Chem., Int. Ed.* **2004,** *43*, (20), 2690-2694; (g) Liu, Y.; Li, X.-Q.; Chen, Y.; Guan, X.-D., *J. Phys. Chem. B* **2004,** *108*, (50), 19541-19549; (h) Liu, Y.; Song, Y.; Chen, Y.; Li, X.-Q.; Ding, F.; Zhong, R.-Q., *Chem.-Eur. J.* **2004,** *10*, (15), 3685-3696; (i) Liu, Y.; Zhao, Y.-L.; Chen, Y.; Ding, F.; Chen, G.-S., *Bioconjugate Chem.* **2004,** *15*, (6), 1236-1245; (j) Liu, Y.; Zhao, Y.-L.; Chen, Y.; Liang, P.; Li, L., *Tetrahedron Lett.* **2005,** *46*, (14), 2507-2511; (k) Liu, Y.; Wang, H.; Chen, Y.; Ke, C.-F.; Liu, M., *J. Am. Chem. Soc.* **2005,** *127*, (2), 657-666; (l) Liu, Y.; Song, Y.; Chen, Y.; Yang, Z.-X.; Ding, F., *J. Phys. Chem. B* **2005,** *109*, 10717-10726; (m) Liu, Y.; Liang, P.; Chen, Y.; Zhao, Y.-L.; Ding, F.; Yu, A., *J. Phys. Chem. B* **2005,** *109*, (49), 23739-23744; (n) Liu, Y.; Kang, S.; Chen, Y.; Cao, R.; Shi, J., *Comb. Chem. High Throughput Screening* **2007,** *10*, (5), 350-357; (o) Liu, Y.; Fan, Z.; Zhang, H.-Y.; Yang, Y.-W.; Ding, F.; Liu, S.-X.; Wu, X.; Wada, T.; Inoue, Y., *J. Org. Chem.* **2003,** *68*, (22), 8345-8352; (p) Liu, Y.; Wu, H.-X.; Chen, Y.; Chen, G.-S., *Supramol. Chem.* **2009,** *21*, (5), 409-415; (q) Rong, D.; D'Souza, V.T., *Tetrahedron Lett.* **1990,** *31*, (30), 4275-4278; (r) Filippone, S.; Heimann, F.; Rassat, A., *Chem. Commun.* **2002**, (14), 1508-1509; (s) Nelissen, H.F.M.; Feiters, M.C.; Nolte, R.J.M., *J. Org. Chem.* **2002**, (67), 5901-5906; (t) Yuan, D.-Q.; Lu, J.; Atsumi, M.; Izuka, A.; Kai, M.; Fujita, K., *Chem. Commun.* **2002**, (7), 730-731; (u) Lecourt, T.; Mallet, J.-M.; P. Sinay, P., *Eur. J. Org. Chem.* **2003**, 4553-4560; (v) Filippone, S.; Rassat, A., *C. R. Chim.* **2003,** *6*, (1), 83-86; (w) Yang, J.; Wang, Y.; Rassat, A.; Zhang, Y.; Sinay, P., *Tetrahedron* **2004,** *60*, (52), 12163-12168; (x) Wang, K.-R.; Guo, D.-S.; Jiang, B.-P.; Sun, Z.-H.; Liu, Y., *J. Phys. Chem. B* **2010,** *114*, (1), 101-106; (y) Zhang, Y.-M.; Chen, Y.; Yang, Y.; Liu, P.; Liu, Y., *Chem.-Eur. J.* **2009,** *15*, (42), 11333-11340; (z) Liu, Y.; Li, L.; Zhang, H.-Y.; Yang, Y.-W.; Ding, F.,

Supramol. Chem. **2004,** *16*, (5), 371-379; (aa) Aime, S.; Gianolio, E.; Palmisano, G.; Robaldo, B.; Barge, A.; Boffa, L.; Cravotto, G., *Org. Biomol. Chem.* **2006,** *4*, (6), 1124-1130; (ab) Yamauchi, K.; Takashima, Y.; Hashidzume, A.; Yamaguchi, H.; Harada, A., *J. Am. Chem. Soc.* **2008,** *130*, (15), 5024-5025; (ac) Zhang, Y.-M.; Chen, H.-Z.; Chen, Y.; Ding, F.; Liu, Y., *New J. Chem.* **2013,** *37*, (5), 1554-1560; (ad) Harada, T.; Pham, D.-T.; Leung, M.H.M.; Ngo, H.T.; Lincoln, S.F.; Easton, C.J.; Kee, T.W., *J. Phys. Chem. B* **2011,** *115*, 1268−1274; (ae) Harada, T.; Giorgio, L.; Harris, T.J.; Pham, D.-T.; Ngo, H.T.; Need, E.F.; Coventry, B.J.; Lincoln, S.F.; Easton, C.J.; Buchanan, G., et al., *Mol. Pharmaceutics* **2013,** *10*, 4481−4490; (af) Wallace, S.J.; TKee, T.W.; Huang, D.M., *J. Phys. Chem. B* **2013,** *117*, 12375−12382; (ag) Casas-Solvas, J.M.; Quesada-Soriano, I.; Carreño-Gázquez, D.; Giménez-Martínez, J.J.; García-Fuentes, L.; Vargas-Berenguel, A., *Langmuir* **2011,** *27*, 9729-9737; (ah) Zhao, Y.; Gu, J.; Chi, S.M.; Yang, Y.C.; Zhu, H.Y.; Wang, Y.F.; Liu, J.H.; Huang, R., *Bull. Korean Chem. Soc. 2008, Vol. 29, No. 11 2119* **2008,** *29*, (11), 2119-2124.

(5) (a) Rawal, G.K.; Zhang, P.; Ling, C.-C., *Org. Lett.* **2010,** *12*, (13), 3096-3099; (b) Lecourt, T.; Blériot, Y.; Auzély-Velty, R.; Sollogoub, M., *Chem. Commun.* **2010** *46*, 2238-2240; (c) Liu, Y.; Li, L.; Li, X.-Y.; Zhang, H.-Y.; Wada, T.; Inoue, Y., *J. Org. Chem.* **2003,** *68*, 3646-3657; (d) Mourer, M.; Hapiot, F.; Tilloy, S.; Monflier, E.; Menuel, S., *Eur. J. Org. Chem. 2008, 5723–5730* **2008**, 5723–5730; (e) Barge, A.; Caporaso, M.; Cravotto, G.; Martina, K.; Tosco, P.; Aime, S.; Carrera, C.; Gianolio, E.; Pariani, G.; Corpillo, D., *Chem. -Eur. J.* **2013,** *19*, 12086 - 12092; (f) Christensen, H.S.; Sigurskjold, B.W.; Frihed, T.G.; Marinescu, L.G.; Pedersen, C.M.; Bols, M., *Eur. J. Org. Chem.* **2011**, 5279-5290; (g) Aime, S.; Gianolio, E.; Arena, F.; Barge, A.; Martina, K.; Heropoulos, G.; Cravotto, G., *Org. Biomol. Chem.* **2009,** *7*, (2), 370-379; (h) Jiang, T.; Li, M.; Lawrence, D.S., *J. Org. Chem.* **1995,** *60*, (22), 7293-7297; (i) Breslow, R.; Zhang, X.; Xu, R.; Maletic, M.; Merger, R., **1996,** *118*, 11678-11679; (j) Fathalla, M.; Neuberger, A.; Li, S.-C.; Schmehl, R.; Diebold, U.; Jayawickramarajah, J., *J. Am. Chem. Soc.* **2010,** *132*, 9966-9967; (k) Kotková, Z.; Kotek, J.; Jirák, D.; Jendelová, P.; Herynek, V.; Berková, Z.; Hermann, P.; Lukes, I., *Chem. -Eur. J.* **2010,** *16*, 10094-10102.

(6) Ogoshi, T.; Harada, A., , . *Sensors* **2008,** *8*, (8), 4961-4982.

(7) Carmona, T.; Mayordomo, N.; Martina, K.; Cravotto, G.; Mendicuti, F., *J. Photochem. Photobiol., A* **2012,** *237*, (0), 38-48.

(8) Cervero, M.; Mendicuti, F., *J. Phys. Chem. B* **2000,** *104*, (7), 1572-1580.

(9) Cravotto, G.; Fokin, V.V.; Garella, D.; Binello, A.; Boffa, L.; Barge, A., *J. Comb. Chem.* **2010,** *12*, 13-15.

(10) (a) Madrid, J.M.; Mendicuti, F., *Appl. Spectrosc.* **1997,** *51*, (11), 1621-1627; (b) Pastor, I.; Di Marino, A.; Mendicuti, F., *J. Photochem. Photobiol., A* **2005,** *173*, (3), 238-247; (c) Pastor, I.; Di Marino, A.; Mendicuti, F., *J. Phys. Chem. B* **2002,** *106*, (8), 1995-2003; (d) Di Marino, A.; Rubio, L.; Mendicuti, F., *J. Incl. Phenom. Macroc. Chem.* **2007,** *58*, (1-2), 103-114; (e) Di Marino, A.; Mendicuti, F., *Appl. Spectrosc.* **2002,** *56*, (12), 1579-1587.

(11) (a) Job, P., *Ann. Chim. Appl.* **1928,** *9*, 113-203; (b) Likussar, W.; Boltz, D.F., *Analytical Chemistry* **1971,** *43*, (10), 1265-1272.

(12) Mendicuti, F., *Trends in Physical Chemistry* **2006,** *11*, 61-77.

(13) (a) Kodaka, M., *J. Phys. Chem.* **1991,** *95*, (6), 2110-2112; (b) Kodaka, M., *J. Am. Chem. Soc.* **1993,** *115*, (9), 3702-3705; (c) Kodaka, M., *J. Chem. Soc., Faraday Trans.* **1997,** *93*, (11), 2057-2059; (d) Kodaka, M., *J. Phys. Chem. A* **1998,** *102*, (42), 8101-8103.

(14) Berova, N.; Nakanishi, K.; Woody, R.W., *Circular Dichroism: Principles and Applications*; Wiley-VCH: 2000.

(15) (a) Harata, K., *Bull. Chem. Soc. Jpn.* **1975,** *48*, (2), 375-378; (b) Harata, K., *Bull. Chem. Soc. Jpn.* **1979,** *52*, (6), 1807-1812.

(16) González-Álvarez, M.J.; Di Marino, A.; Mendicuti, F., *J. Fluoresc.* **2009,** *19*, (3), 449-462.

(17) O'Connor, D.V.; Ware, W.R.; Andre, J.C., *J. Phys. Chem. B* **1979,** *83(10)*, 1333-1343.

(18) Lakowicz, J.R., Time-Domain Lifetime Measurements. In *Principles of Fluorescence Spectroscopy*; 3rd ed.; Springer: New York, 2008; p 97.

(19) Lakowicz, J.R., Fluorescence anisotropy. In *Principles of Fluorescence Spectroscopy*; third ed.; Springer: New York, 2006; p 353.

(20) Lakowicz, J.R., Quenching of Fluorescence. In *Principles of Fluorescence Spectroscopy*; third ed.; Springer: New York, 2006; p 278.

(21) *SybylX 2.0*, Tripos International, 1699 S Hanley Road: St Louis, MO, 63144 USA, 2013.

(22) Clark, M.; Cramer, R.D., III; Van, O.N., *J. Comput. Chem.* **1989,** *10*, (8), 982-1012.

(23) MOPAC(AM1) *Included in the Sybyl X2.0 package.*

(24) Brunel, Y.; Faucher, H.; Gagnaire, D.; Rassat, A., *Tetrahedron* **1975,** *31*, (8), 1075-1091.

(25) Blanco, M., *J. Comput. Chem.* **1991,** *12*, (2), 237-247.